Soil Dynamics and Earthquake Engineering 97 (2017) 289–303

Contents lists available at ScienceDirect

Soil Dynamics and Earthquake Engineering

journal homepage: www.elsevier.com/locate/soildyn

Near-field effects on site characterization using MASW technique

Narayan Roy[a], Ravi S. Jakka[b,*]

[a] Department of Civil Engineering, Jadavpur University, Kolkata, India
[b] Department of Earthquake Engineering, Indian Institute of Technology Roorkee, India

ARTICLE INFO

Keywords:
Rayleigh wave dispersion
Near-field effects
Active tests
Passive tests
Finite element method

ABSTRACT

The application of Multichannel Analysis of Surface Wave (MASW) technique is increasing in geotechnical engineering to characterize near surface materials. The dispersion property of Rayleigh wave is utilized in MASW method. MASW often suffers from near-field effects which may result in either underestimation or overestimation of Rayleigh wave phase velocity due to the body waves contamination near to the source. In this paper, a detailed numerical study has been carried out to examine the near-field effects considering three different types of typical S-wave velocity models with four different impedance scenarios in each case. The study shows that the impedance contrast between the half-space and overlying soil layer is having a considerable effect on the underestimation of phase velocity. These near-field effects are also found to be influenced by the type of the S-wave velocity model as well as far and near offset distances. With the increase of impedance contrast, the level of underestimation seems to increase at lower normalized array centre distance due to mode jump. However, such jump can not be observed with limited far offset distances generally used in usual practice due to poor resolution in the dispersion spectra. Significant near-field effect are observed for lower far offset distances and inversely dispersive S-wave velocity models. Underestimation of Rayleigh wave phase velocity is quantified in terms of two normalized parameters. Finally, a field study is also conducted to verify our numerical findings.

1. Introduction

MASW is widely used for geotechnical site characterization to extract the shear wave velocity variation with depth. Shear wave velocity which is further used to calculate the design ground motion at the surface level, is most important parameter for earthquake geotechnical engineering related studies. Hence, the accuracy of the test and its proper interpretation is very much essential for reliable estimation of shear wave velocity profiles. The applications of surface waves for engineering problems started in the 1950s with the Steady State Rayleigh Method [13], but their wide spread development have arrived only in the last two decades with the proposition of the Spectral Analysis of Surface wave (SASW) method [19] and the Multichannel Analysis of Surface wave (MASW) method [18,21,30]. Surface wave method uses the dispersive nature of Rayleigh wave with the assumption that the wavefield is purely of plane Rayleigh waves. However, when we use a linear array to capture a signal generated by an active source placing it very close to the first geophone, the assumption of plane Rayleigh wave may not holds true. The wave field actually consists of both cylindrically propagating Rayleigh wave and body waves [22,34]. So, consideration of plane Rayleigh wave propagation may results in erroneous measurement of Rayleigh wave dispersion, which is termed as near-field effects. Generally, near-field effects cause the underestimation of Rayleigh-wave phase velocity at low frequencies [4,23,27,33].

Several studies have been carried out to mitigate near-field effects and some filtering criteria were proposed based on the ratio of source-to-first receiver distance and Rayleigh wavelength for two receivers case in Spectral Analysis of Surface Wave (SASW) testing [8,9,11,25]. Their study recommended the filtering criteria, i.e., the ratio of $R_1/\lambda_R >$ (1/3 to 2) for a particular ratio of $\Delta R/R_1(=1)$, where R1 is near offset distance, λ_R Rayleigh wavelength, and ΔR is the distance between receivers. But in the case of Multichannel Analysis of Surface Wave (MASW) the scenario is little different from the two receivers, i.e., SASW case. Very few studies have been conducted to investigate the near-field effects for multistation surface wave methods. Zywicki and Rix [35] proposed an advance signal processing technique to analyze the surface wave field data. They proposed cylindrical beamforming technique over conventional plane wave beamformer to separate out the cylindrically spreading Rayleigh wave over plane wave approximation. Xu et al. [31] estimated minimum offset for multichannel surface wave survey to avoid near-field effects. They found out near-offset varies with the ratio of V_P/V_S and the thickness of the first layer. Multi-Offset Phase Analysis (MOPA) has also been proposed to extract the

* Corresponding author.
E-mail addresses: narayan.roy04@gmail.com (N. Roy), rsjakka@gmail.com (R.S. Jakka).

http://dx.doi.org/10.1016/j.soildyn.2017.02.011
Received 17 August 2015; Received in revised form 12 February 2017; Accepted 26 February 2017
0267-7261/

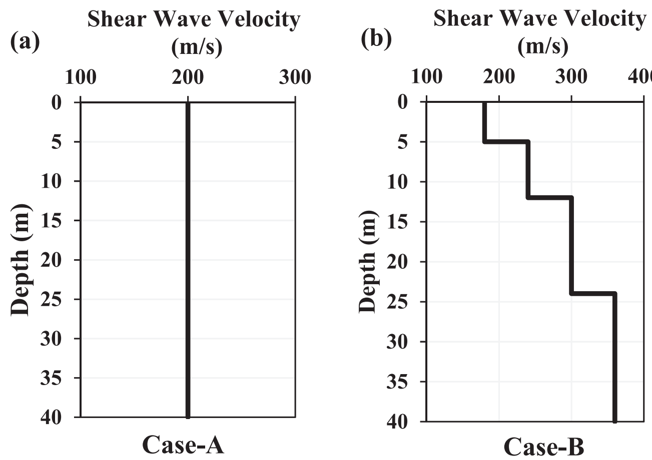

Fig. 1. S-wave velocity models used in validation purpose.

Table 1
Details of soil profiles for validation.

Thickness (m)	Case-A (m/s)	Case-B (m/s)	Poisson's Ratio, ν	Density, ρ (t/m^3)
5	200	180	0.3	1.8
7		240	0.3	1.8
12		300	0.3	1.8
Half-space		360	0.3	1.8

actual information in the dispersion analysis of surface wave data [27]. But because of the simplicity and computational efficiency most of the processing techniques still prefer to use the plane-wave consideration [20]. Yoon and Rix [33] investigated the near-field effects and found out that the Rayleigh wave phase velocity is underestimated at lower frequencies. It becomes more significant when the S-wave velocity models are inversely dispersive. They quantified the error due to near-field effects with respect to normalized array centre distance. Bodet et al. [4] also drew the similar kind of conclusion about the under-estimation of phase velocity at low frequency region. They concluded that phase underestimation becomes significant (≥5%) when the measured wavelength crosses the 50% of spread length. Aung and Leong [1] simulated the near-field effects using finite element modelling and they observed that the Rayleigh-wave phase velocity can be accurately estimated beyond 40 Hz frequency irrespective of far offset

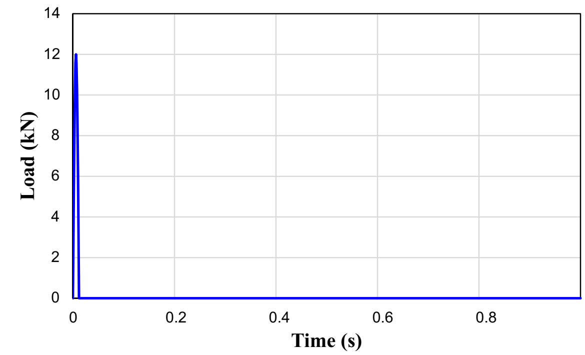

Fig. 3. Half-sine pulse used to model the impulse loading.

distances or near offset distance. However, below 40 Hz frequency, near-field effects may results in underestimation or over estimation of phase velocity. Li and Rosenblad [16] conducted a study to assess the influence of source-to-receiver offset distance on the measured surface wave phase velocity from experimental field studies at eleven deep soil sites in the Mississippi embayment of the central United States. Authors concluded that the influence of near-field effects is clearly evident while the normalized source-to-receiver offset is kept 0.5 or less.

So, it is very much required to accurately asses the level of influence of underestimation or overestimation for proper characterization of a geotechnical site and to increase the reliability of surface wave dispersion measurements. The studies on different uncertainties of surface wave methods have been performed by different researchers to increase the accuracy of the extracted velocity profiles [3,10,12,24] but only few studies have been carried out on near-field effects. So far the studies on near-field effects are confined only for limited type of S-wave velocity models. In this paper, we have studied the near-field effects using Finite Element modelling for different kinds of S-wave velocity models with varying impedance contrasts. Impedance contrast between the half-space and overlying soil layer may vary from site to site. In case of deep alluvium deposits, slow increase of shear-wave velocity is generally observed and there exists no sharp impedance contrast. But for a shallow bedrock, a sharp impedance contrast exists between the half-space and the overlying layer. Here, we simulated the near-field effects for a wide range of impedance contrast scenarios between the half-space and the soil layer to get a more clear insight on the quantification of the error due to near-field effects for different types

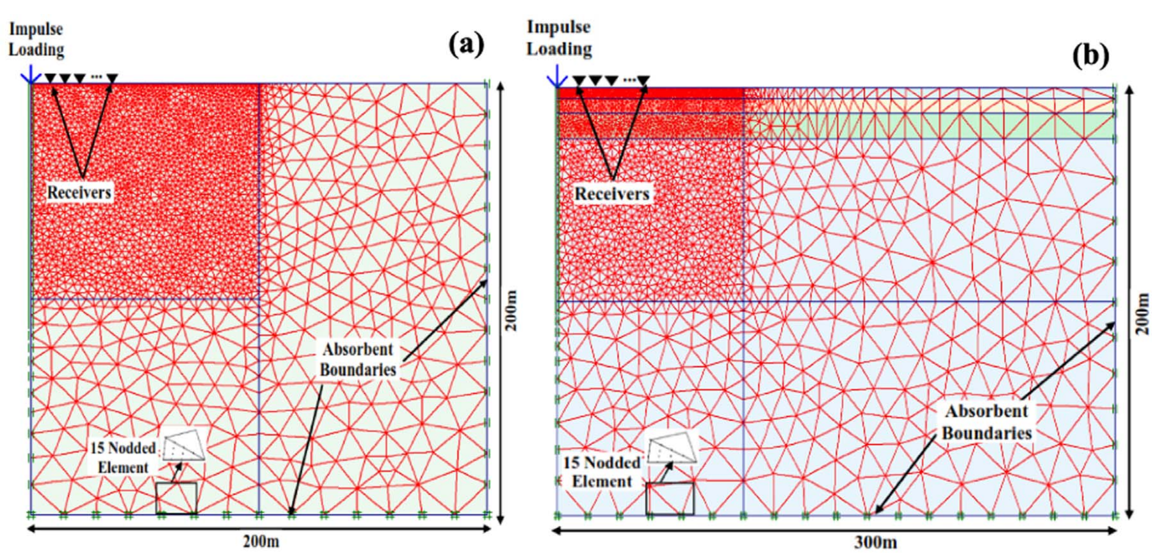

Fig. 2. Numerical model details for 2D FE model (a) Homogeneous case (Case-A), and (b) Layered profile case (Case-B).

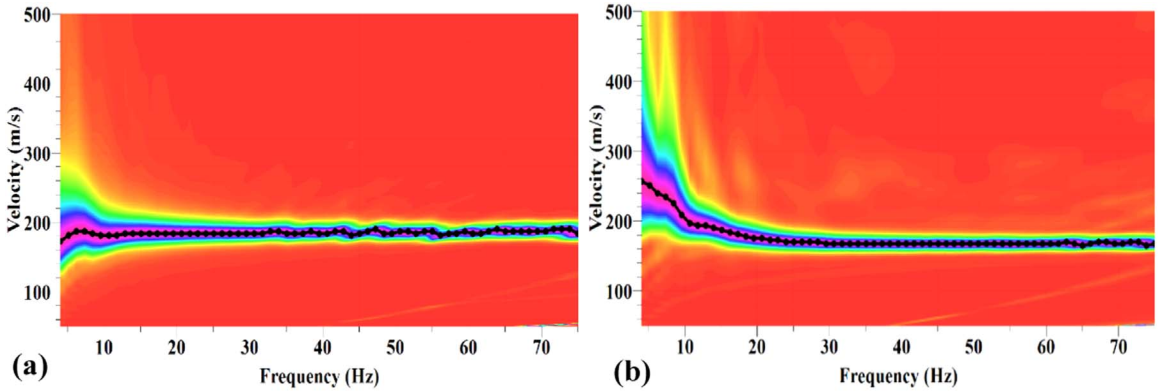

Fig. 4. Dispersion curves after frequency-wavenumber analysis; (a) Homogeneous half-space (Case-A), and (b) Normally dispersive soil profile (Case-B).

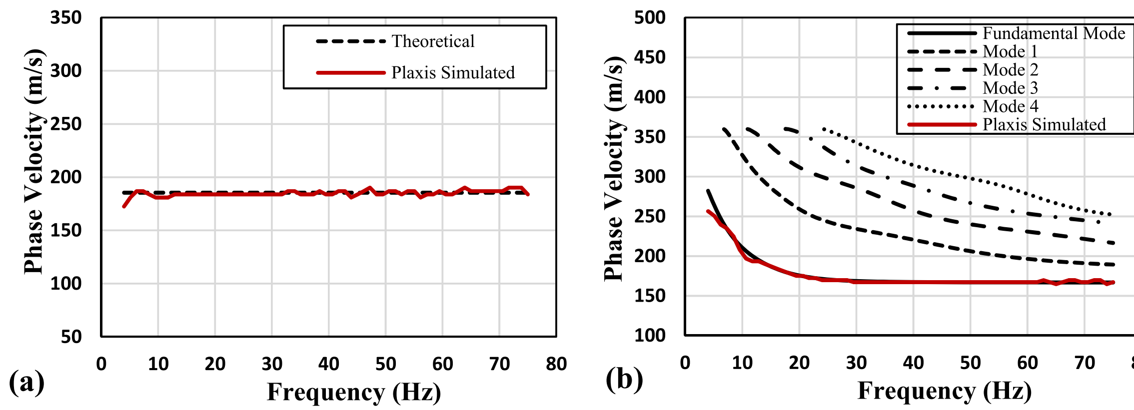

Fig. 5. Comparison of dispersion curves from PLAXIS and modal dispersion curves; (a) Homogeneous case (Case-A), and (b) Layered soil case (Case-B).

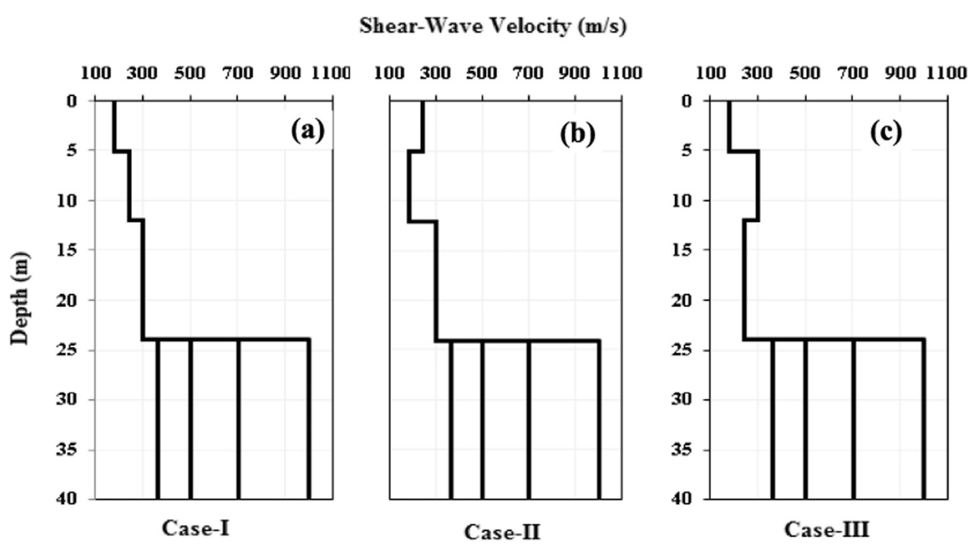

Fig. 6. S-wave velocity models considered for numerical simulation; (a) Normally dispersive, (b) Inversely dispersive with soft layer, and (c) Inversely dispersive with stiff layer.

Table 2
Details of soil layer properties (**Case-I**).

Thickness (m)	Case-I					
	I(a) V_S (m/s)	I(b) V_S (m/s)	Density, ρ (kN/m^3)	I(c) V_S (m/s)	I(d) V_S (m/s)	Density, ρ (kN/m^3)
5	180	180	18.0	180	180	18.0
7	240	240	18.0	240	240	18.0
12	300	300	18.0	300	300	18.0
Half-space	360	500	18.0	700	1000	20.0

Table 3
Details of soil layer properties (**Case-II**).

Thickness (m)	**Case-II**					
	II(a) V_S (m/s)	**II(b)** V_S (m/s)	Density, ρ (kN/m^3)	**II(c)** V_S (m/s)	**II(d)** V_S (m/s)	Density, ρ (kN/m^3)
5	240	240	18.0	240	240	18.0
7	180	180	18.0	180	180	18.0
12	300	300	18.0	300	300	18.0
Half-space	360	500	18.0	700	1000	20.0

Table 4
Details of soil layer properties (**Case-III**).

Thickness (m)	**Case-III**					
	III(a) V_S (m/s)	**III(b)** V_S (m/s)	Density, ρ (kN/m^3)	**III(c)** V_S (m/s)	**III(d)** V_S (m/s)	Density, ρ (kN/m^3)
5	180	180	18.0	180	180	18.0
7	300	300	18.0	300	300	18.0
12	240	240	18.0	240	240	18.0
Half-space	360	500	18.0	700	1000	20.0

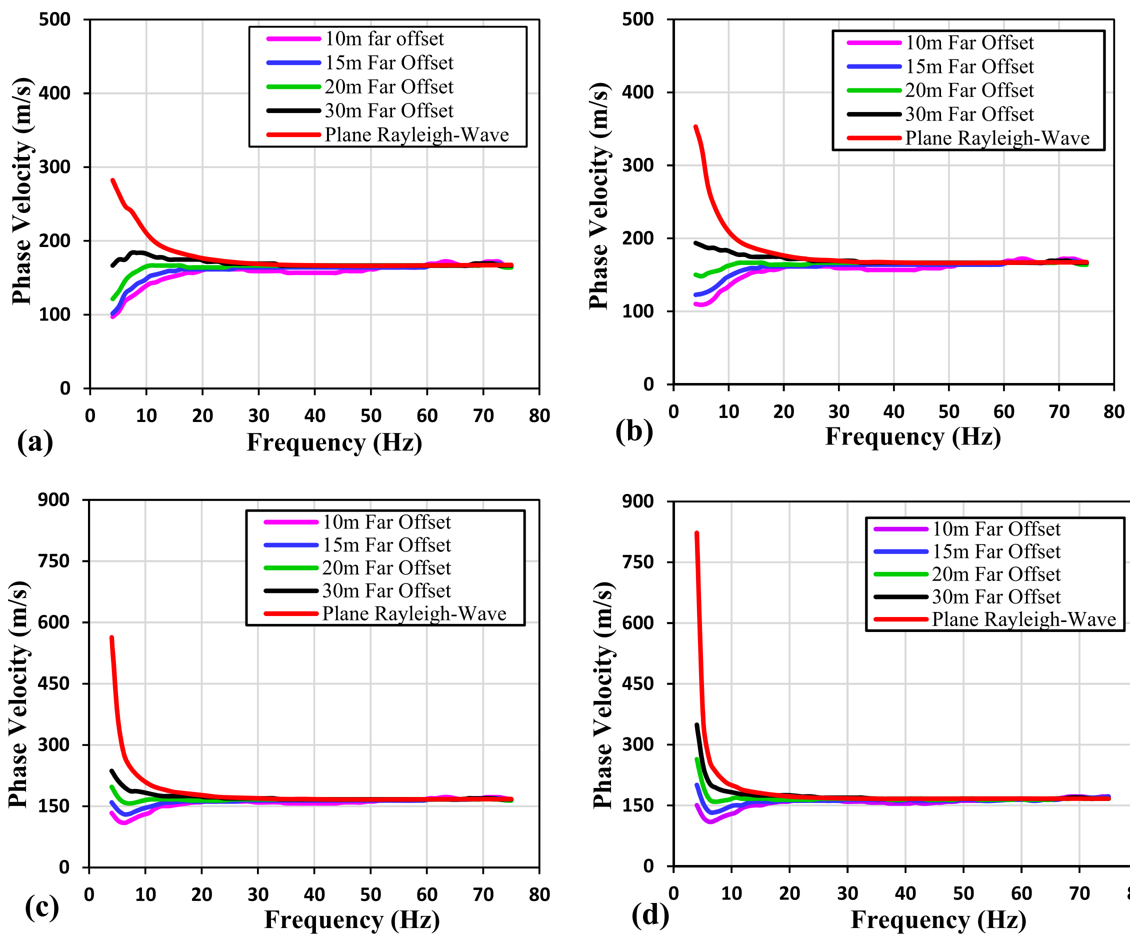

Fig. 7. Comparison of dispersion curves for full-wave field for Case-I S-wave velocity model with a half-space velocity of; (a) HS-360, (b) HS-500, (c) HS-700, and (d) HS-1000 m/s.

of S-wave velocity models. A site specific field study has also been conducted to verify our numerical findings.

2. Methodology

A numerical simulation is performed to simulate the effect of velocity contrast between the half-space and overlying soil layer for three typical types of S-wave velocity models on near-field effects. The simulation mainly considers two different scenarios of surface wave propagation, first to model the wave propagation for full wave field due to a point load on the surface and second, to model the wave propagation purely for Rayleigh wave, i.e., only surface wave in a layered medium. PLAXIS Finite Element program [5] is used to model the wave propagation for full wave field due to an impulse loading,

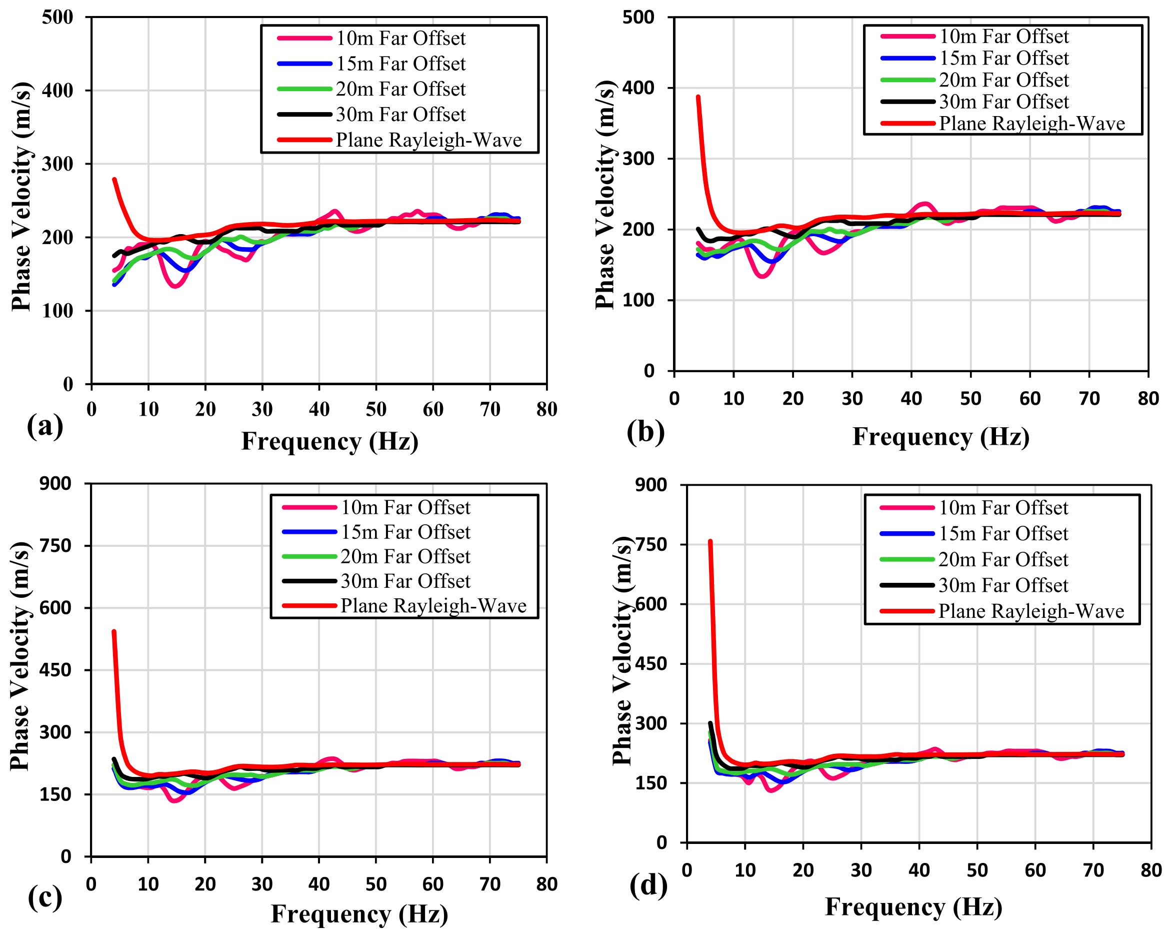

Fig. 8. Comparison of dispersion curves for full-wave field for Case-II S-wave velocity model with a half-space velocity of; (a) HS-360, (b) HS-500, (c) HS-700, and (d) HS-1000 m/s.

whereas Mat_disperse, a matlab program written by Glenn J. Rix is used to model motions due to plane Rayleigh waves. Mat_disperse can also be used to calculate effective phase velocity at each receiver location for a layered, linear elastic half-space by the superposition of multiple modes of plane Rayleigh waves and does not include contributions from body waves [15]. Here, we generated the effective phase velocity at each receiver location for the considered S-wave velocity model to generate the plane Rayleigh wave dispersion curve, which is sometimes called apparent dispersion curve. Using PLAXIS Finite Element program, surface wave is modelled for full wave field and finally dispersion curve is generated using frequency-wavenumber analysis. The dispersion curves for full wave field are generated for similar array configuration to compare it with the plane Rayleigh dispersion curve and to quantify the errors. Errors due to near-field effects are expressed in terms of two normalized parameters proposed by Yoon and Rix [33]. Finally, a field study is conducted to simulate the near-field effects experimentally. Active and passive surface wave tests are carried out at Nehru stadium site at Roorkee city. Passive surface wave tests are used for the study of plane Rayleigh wave case and active source surface wave tests are used for the study of full-wave field case. Passive data has been analyzed using SPAC (Spatial Auto-Correlation) method. The spatial auto-correlation technique takes the advantage of the random distribution of passive sources in time and space to link auto-correlation ratios to phase velocities, and finally near-field effects are quantified in terms of two normalized parameters.

2.1. Full wavefield modelling

PLAXIS Finite Element program is used to model the surface wave for full wave field due to an point load acting on the free surface. The equation of motion of a N degrees of freedom system subjected to an impact loading can be written as follows:

$$M\ddot{u}(t) + C\dot{u}(t) + Ku(t) = F(t) \tag{1}$$

where M, C and K are the N×N mass, damping and stiffness matrixes, respectively. $\ddot{u}(t)$, $\dot{u}(t)$ and $u(t)$ are the acceleration, velocity and displacement vectors, respectively. The applied impulsive force is $F(t)$. By using the implicit time integration scheme of Newmark, the displacement and the velocity at the point in time $(t + \Delta t)$ can be expressed as

$$u^{t+\Delta t} = u^{t} + \dot{u}^{t}\Delta t + \left(\left(\frac{1}{2} - \alpha\right)\ddot{u}^{t} + \alpha\ddot{u}^{t+\Delta t}\right)\Delta t^{2} \tag{2}$$

$$\dot{u}^{t+\Delta t} = \dot{u}^{t} + ((1-\beta)\ddot{u}^{t} + \beta\ddot{u}^{t+\Delta t})\Delta t \tag{3}$$

where Δt is the time step, α and β are the Newmark's parameters which determine the accuracy of the numerical time integration. For a stable solution, the following conditions should satisfy

$$\beta \geq 0.5 \text{ and } \alpha \geq 0.25(0.5 + \beta)^{2} \tag{4}$$

So, the dynamic problem is solved with the help of a 2D axisymmetric model using finite element method implemented in PLAXIS computer program package. Vertical particle motion velocities have been computed at several positions from the source for further processing. Special absorbant boundaries have been provided at the boundaries to avoid the spurious reflections of the waves from the model boundaries. These boundaries are introduced based on the Lysmer-Kohlmeyer model [17]. According to this model, the normal and shear stress components absorbed by providing a damper, which can be determined as follows:

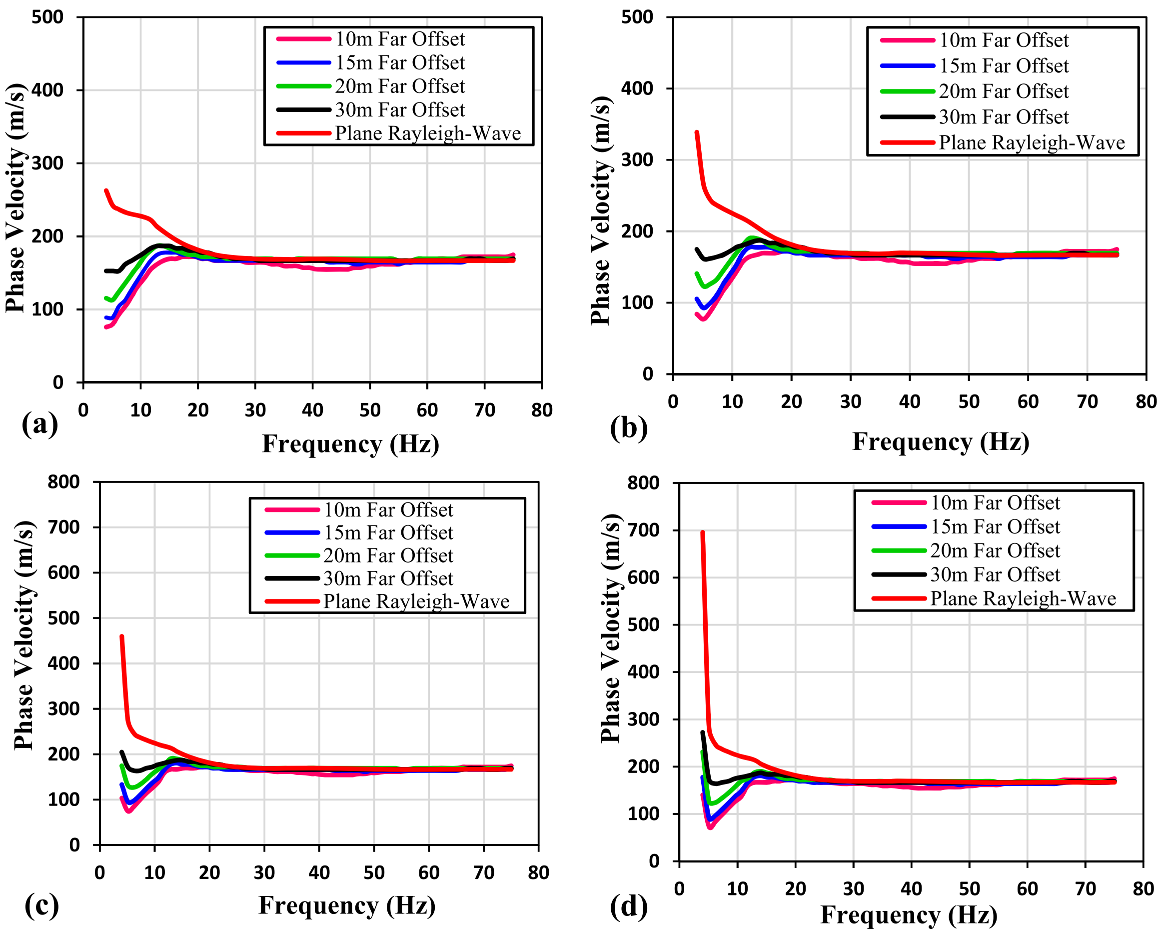

Fig. 9. Comparison of dispersion curves for full-wave field for Case-III S-wave velocity model with a half-space velocity of; (a) HS-360, (b) HS-500, (c) HS-700, and (d) HS-1000 m/s.

$$\sigma_n = -C_1 \rho V_P \dot{u}_x \quad (5)$$

$$\tau = -C_2 \rho V_S \dot{u}_y \quad (6)$$

where ρ is the mass density, V_S is the shear wave velocity, V_P is the longitudinal wave velocity, $\dot{u}_x$ and $\dot{u}_y$ are the velocity of particle motion in the direction of x and y, respectively, and C_1 and C_2 are relaxation coefficients used to improve the wave absorption at the boundaries. C_1 corrects the dissipation in the direction normal to the boundary and C_2 in the tangential direction. A value of C_1=1 and C_2=0.5 results in better absorption of waves. Impulse loading is simulated using a half-sine pulse acting for short duration. The load is acting for a short duration of 0.012 s with a peak load of 12 kN. Total time duration of the simulation has been kept 1 s with a time step of 0.001 s.

2.2. Validation of FE model

Before starting the main simulation for different types of S-wave velocity models, it is necessary to validate the models. For this purpose, two different axisymmetric models representing different types of S-wave velocity models (Fig. 1) have been prepared in finite element using PLAXIS program. Case-A is homogeneous half-space with a constant velocity of 200 m/s (Table 1), and Case-B is a normally dispersive profile with three layers above half-space. The details about the profiles are presented in Table 1. Poisson's ratio and density are kept constant for all cases as these parameters are having very little effects on Rayleigh wave dispersion [26,32].

Fig. 2 shows the developed finite element model for homogeneous (Fig. 2a) and layered case S-wave velocity model (Fig. 2b). Meshes are refined up to 100 m×100 m dimensions to accurately simulate the surface waves based on the distance of interests from the source and greater than one wavelength depth. This refinement will help to accurately measure the velocity time histories for higher frequencies at surface level. To reduce the computational time, the size of meshing is kept little bigger beyond this dimension without hindering the accuracy of the computation. The size of the models has been decided based on the minimum frequency and maximum possible velocity of the model, i.e., the longest wavelength information that will be computed from the analysis. Aung and Leong [2] proposed a criterion for numerical modelling using finite element to avoid the numerical errors because of the reflection of waves from the boundaries. They proposed that the model size should be twice the longest wavelength available to avoid the discrepancies. Here, our minimum frequency (f_{min}) that we extracted from the simulation is 4 Hz and the velocity of the half-space 200 m/s and 360 m/s for Case-A and Case-B, respectively. So the maximum extracted wavelengths (λ_{max}) are 50 m and 90 m. Based on the criterion, the size of the model should be 100 m and 180 m for Case-A and Case-B, respectively. Here, for more accurate results we kept the size of the model as 200 m×200 m and 300 m×200 m. Surface wave is modelled due to an impulse loading on the surface as shown in Fig. 3. Absorbent boundaries are introduced at bottom and right hand side of a PLAXIS model. Particle velocity time histories have been generated at 1 m interval for a near offset distance of 1 m. At total 96 receiver positions velocity time histories have been generated with a far offset of 96 m for both the homogeneous and layered soil profile cases in the validation.

After generating the seismogram of velocity time histories at 96 receiver locations, these data are further processed to generate the dispersion spectra to extract the dispersion curve. For this purpose, Geopsy program package [29], which uses the frequency-wavenumber

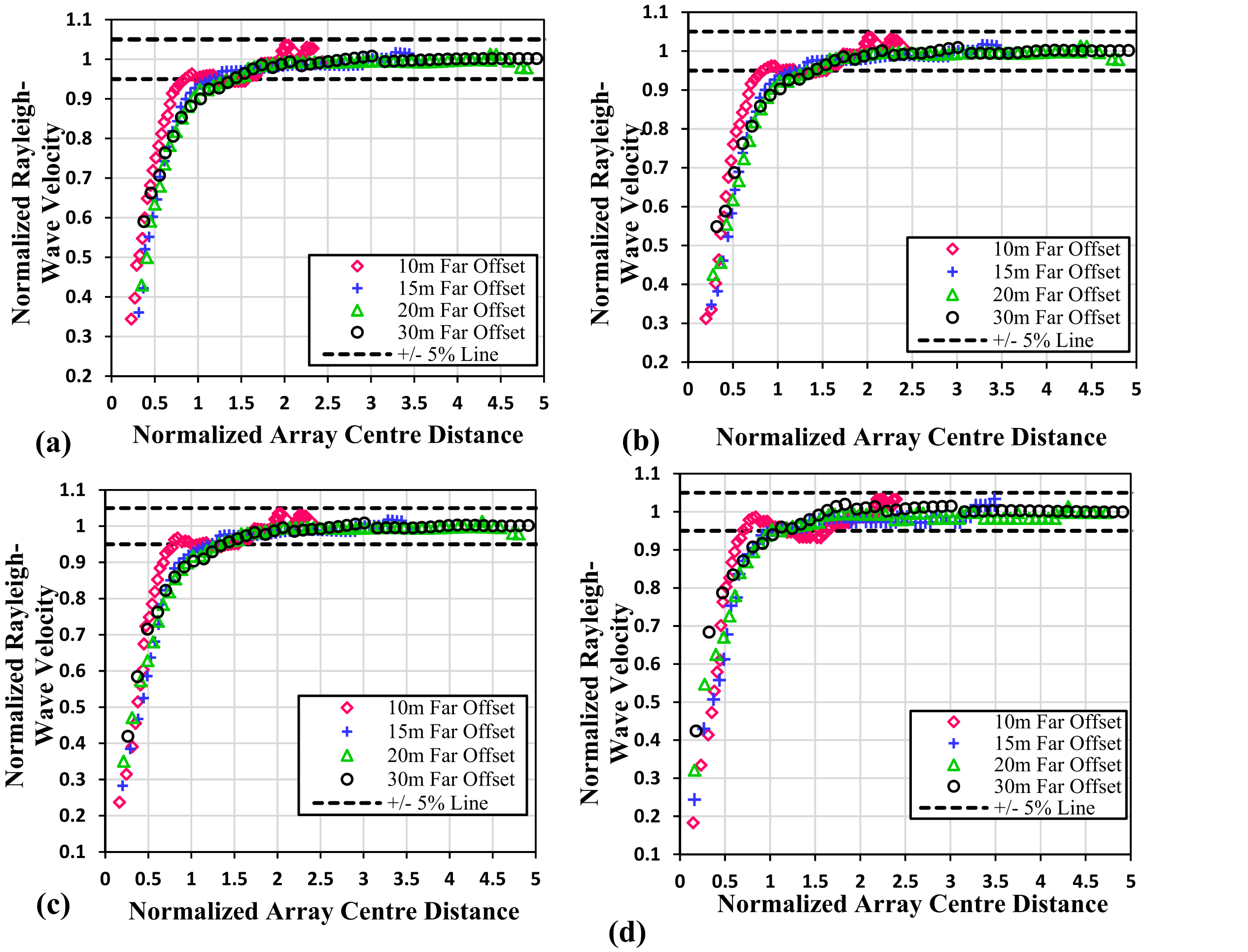

Fig. 10. Near-field effects for Case-I S-wave velocity models with a half-space velocity of; (a) HS-360, (b) HS-500, (c) HS-700, and (d) HS-1000 m/s.

(*f-k*) method is used to analyze the data. Dispersion curves are generated in a frequency range from 4 Hz to 75 Hz, which is mainly associated with the frequency range of engineering interests. Fig. 4 presents the dispersion image for homogeneous S-wave velocity model (Fig. 4a) and normally dispersive S-wave velocity model (Fig. 4b). The dispersion image clearly depicts the concentration of energy which represents the Rayleigh-wave phase velocity at different frequency values. A total 65 points are selected to calculate the phase velocity between a frequency ranges from 4 Hz to 75 Hz. Our simulated dispersion curves have been compared with the theoretical modal dispersion curves. Modal dispersion curves (Theoretical dispersion curves) have been generated using modified algorithm of Thomson [28] and Haskell [7] by Dunkin [6] and Knopoff [14].

The comparison of results is presented in Fig. 5 for homogeneous S-wave velocity model (Fig. 5a) and normally dispersive S-wave velocity model (Fig. 5b). PLAXIS simulated dispersion curve is superimposed with the respective theoretical modal dispersion curves so as to make a proper comparison to validate the PLAXIS results. The comparison exhibits an excellent agreement between the dispersion curve obtained from the PLAXIS simulation and theoretical dispersion curve. The agreement is excellent at higher frequencies but the dispersion curve generated by PLAXIS simulation shows a little downward trend at lower frequencies. This is expected as the Rayleigh-wave phase velocity is underestimated at lower frequencies in PLAXIS simulation due to near-field effects. PLAXIS models the wave propagation for full wavefield, whereas theoretical dispersion curve stands for plane Rayleigh wave propagation. This is quantified later to estimate the level of underestimation due to near-field effects. So, the differences at lower frequencies are mainly arising because of the underestimation of Rayleigh wave phase velocity while producing the surface wave using a point source.

2.3. Near-Field effects simulation

Numerical simulations have been performed to asses the effect of the impedance contrast on near-field effect using different types of S-wave velocity models. Three typical S-wave velocity models have been used with four different impedance scenarios. Fig. 6 shows the considered profiles with four different half-space velocities. Case-I is normally dispersive S-wave velocity model (Fig. 6a), Case-II is inversely dispersive S-wave velocity model with soft layer trapped between two hard layers (Fig. 6b) and Case-III represents inversely dispersive profile with a hard layer between two soft soil layers (Fig. 6c).

The properties and layering information are provided in Tables 2–4. Poisson's ratio 0.3 has been used for all the layers. Damping ratio is set to zero as the effect of damping ratio on near-field effects is negligible [32]. Case-I S-wave velocity model is further subdivided into Case-I(a), Case-I(b), Case-I(c) and Case-I(d) with a half-space velocity of 360 m/s, 500 m/s, 700 m/s and 1000 m/s, respectively. Table 2 shows the details about the layering information for Case-I S-wave velocity model. Similarly, Case-II (Table 3) and Case-III (Table 4) S-wave velocity models are also subdivided into four different impedance cases. Density for Case-I(a) & (b), Case-II(a) & (b) and Case-III(a) & (b) have been kept 18 kN/m^3, and for Cases I(c) & (d), Case-II(c) & (d) and Case-III(c) & (d) have been kept 20 kN/m^3.

These S-wave velocity models are modelled in PLAXIS Finite Element program similar to validation cases. The size of the models

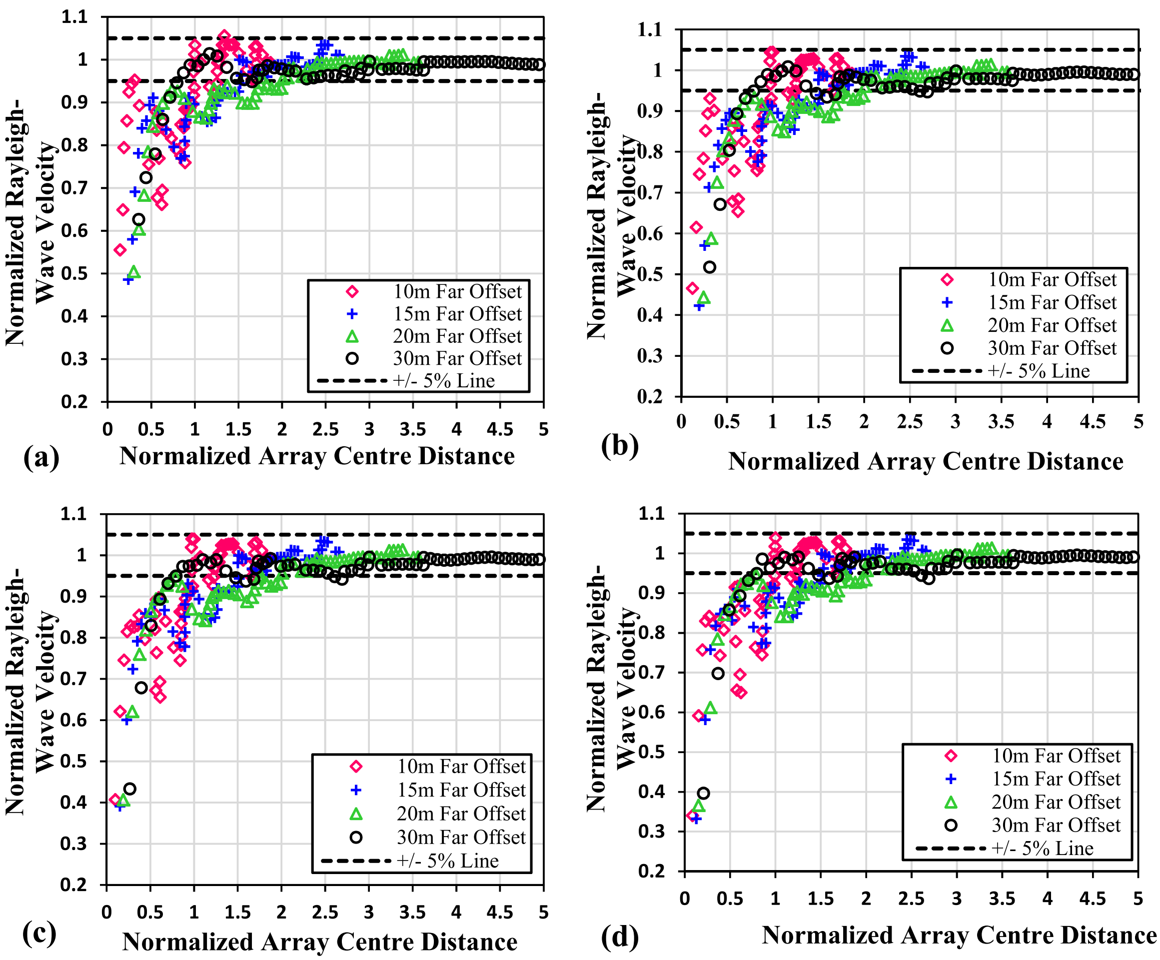

Fig. 11. Near-field effects for Case-II S-wave velocity models with a half-space velocity of; (a) HS-360, (b) HS-500, (c) HS-700, and (d) HS-1000 m/s.

have been fixed based on the maximum available wavelength. Minimum wavelength to domain size ratio is always maintained minimum (0.5) so as to avoid the numerical errors in the simulations. Absorbant boundaries are introduced at the right end and bottom to avoid the reflection from the boundaries. The similar half-sine pulse used earlier in validation cases has been used as an impulsive source with a duration of 0.012 s. These generated signals are sampled at different locations from the source, which we can termed as the receiver positions. Velocity time histories are generated with a source-to-first receiver distance 1 m as well as and receiver-to-receiver distances of 1 m.

3. Results of the simulation

The dispersion curves have been developed for full wave field and plane Rayleigh wave cases. Four different 10, 15, 20 and 30 m far offset configurations have been used to present the results of the numerical simulations. Source-to-first receiver distances, i.e. near offset distances and inter receiver spacing have been kept 1 m. Fig. 7 shows the comparison of the dispersion curves for Case-I S-wave velocity model, i.e., normally dispersive. Fig. 7a–d show the comparison of the dispersion curve of full-wave field for Case-I(a), Case-I(b), Case-I(c) and Case-I(d) cases, respectively. In each figure, a reference plane Rayleigh wave curve for 30 m far offset case has also been superimposed just to show the level of underestimation. It is very much evident from the figures that the level of underestimation is very much prominent for high impedance cases (Fig. 7d). As the far offset distances increases, full-wave dispersion curve reaches closer to the actual velocity, i.e. plane Rayleigh wave velocity, and the level of underestimation rises while the far offset distances are reduced.

For Case-II S-wave velocity model, i.e., for inversely dispersive profile with soft layer, the comparison of dispersion curves for full-wave field is presented in Fig. 8. Fig. 8a–d show the result for the cases Case-II(a), Case-II(b), Case-II(c) and Case-II(d), respectively. Here, we can observe the participation of higher mode as an upward trend in all the dispersion curves is observed at higher frequencies. Similar kind of higher underestimation in phase velocity as seen in case of I(d), is observed for Case-II(d) as well (high impedance profile). Underestimation is also quite higher for low far offset distances, which can be observed clearly in all the considered S-wave velocity model cases. Fig. 9 shows the results of inversely dispersive S-wave velocity model with hard layer between two soft layers. Here, we can also observe the gradual reduction in the level of underestimation with the increase in the far offset distances.

Now, effective dispersion curves for plane Rayleigh wave are simulated using Mat_disperse program for 10, 15, 20 and 30 m far offset distances so as to make a direct comparison with similar offset configuration of PLAXIS simulated cases and to quantify the error due to near-field effects. Near-field effects have been represented in terms of two normalized parameters proposed by Yoon and Rix [33], namely normalized array centre distance and normalized Rayleigh wave velocity. Normalized array centre distance can be written as follows

$$\frac{\bar{x}}{\lambda_R} = \frac{\frac{1}{N}\sum_{n=1}^{N} x_n}{\lambda_R} = \frac{(\frac{1}{N}\sum_{n=1}^{N} x_n)f}{V_R}$$

where, $\bar{x}$ is the mean distance of all receivers in an array with respect to the source, λ_R is the wavelength of the Rayleigh wave, N is number of channels in an array, x_n is the distance of the nth receiver from the

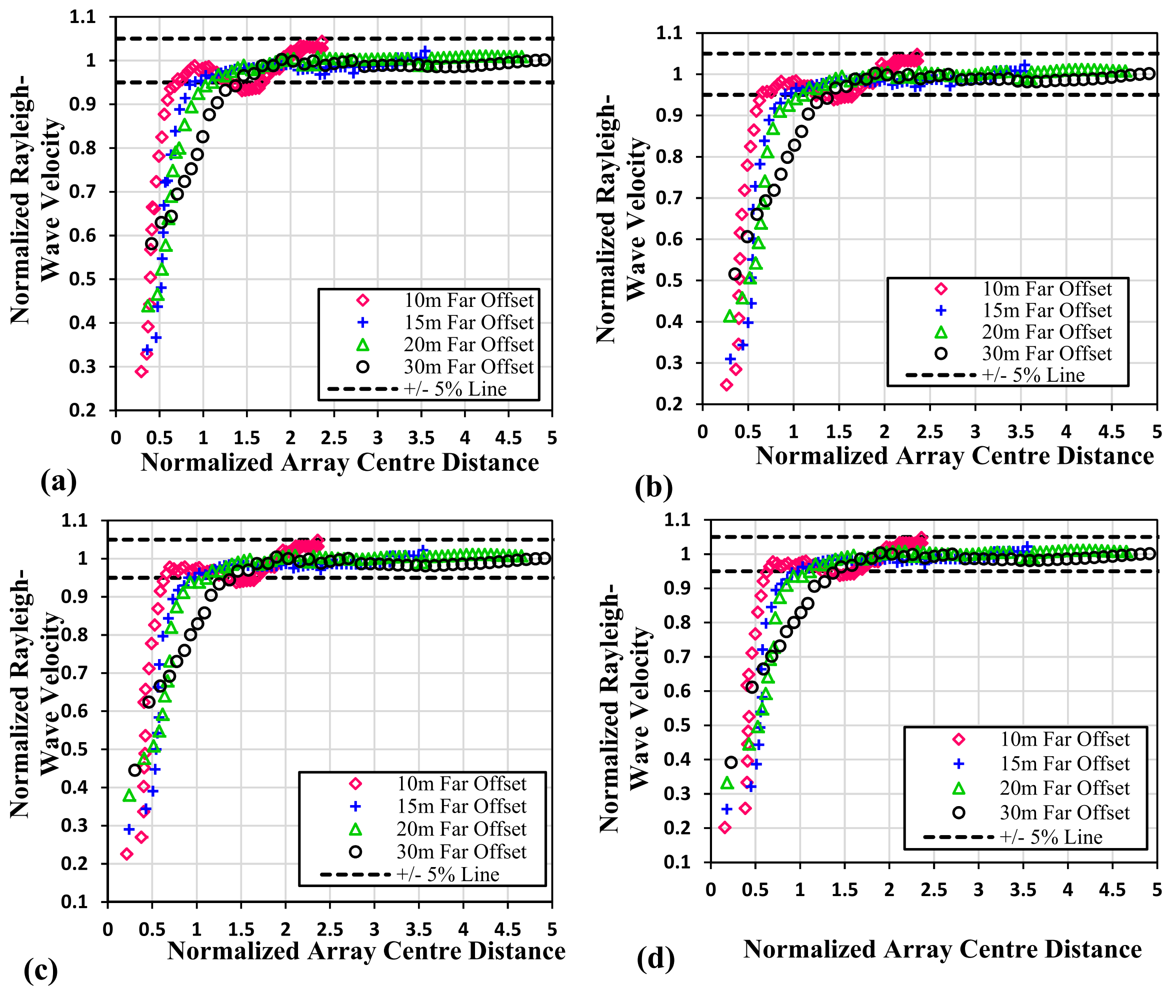

Fig. 12. Near-field effects for Case-III S-wave velocity models with a half-space velocity of; (a) HS-360, (b) HS-500, (c) HS-700, and (d) HS-1000 m/s.

Table 5
Underestimation of Rayleigh wave velocity due to near-field effects.

Normalized Array Centre Distance	Case-I				Case-II				Case-III			
	Case-I(a)	Case-I(b)	Case-I(c)	Case-I(d)	Case-II(a)	Case-II(b)	Case-II(c)	Case-II(d)	Case-III(a)	Case-III(b)	Case-III(c)	Case-III(d)
1	0.9	0.9	0.9	0.93	0.86	0.88	0.86	0.86	0.84	0.84	0.84	0.87
1.5	0.94	0.94	0.95	0.92	0.9	0.9	0.9	0.9	0.93	0.94	0.94	0.94
2	0.98	0.98	0.98	0.96	0.95	0.95	0.95	0.95	0.98	0.98	0.98	0.96

source, V_R is the Rayleigh wave phase velocity, and f is the frequency.

Normalized Rayleigh wave velocity is expressed as below

$$\frac{V_R}{V_{R,\quad Plane}}$$

where V_R is Rayleigh wave phase velocity considering near-field effects and $V_{R,Plane}$ is the plane Rayleigh wave velocity, i.e., without near-field effects. The results due to near-field effects are plotted considering the normalized Rayleigh wave velocity on y-axis and normalized array centre distance on x-axis. Fig. 10 represents the near-field effects for Case-I S-wave velocity model, i.e. normally dispersive profile in terms of the above mentioned normalized parameters. These two parameters are selected mainly because it results in a plot which is independent of far offset distances and follows a unique trend so that a direct comparison is possible for different receiver scenarios.

It is very much evident from the Fig. 10 that the underestimation increases as impedance contrast increases (Fig. 10a–d). In this normally dispersive case, a little high scatter in the data is observed for high impedance contrast profile (Fig. 10d). Far offset distances are having a pronounced effect in the underestimation, lower is the underestimation for higher far offset distances. For all the impedance cases, it is observed that with a normalized array centre distance 1, the underestimation reduces dramatically and leads to a better estimate of Rayleigh wave phase velocity. Fig. 11 shows the inversely dispersive soil case with a soft layer trapped between hard layers. Here, scatter in the data is quite noticeable and it leads to significant near-field effects.

It is observed from Case-II that the underestimation of Rayleigh wave phase velocity is very high for high impedance case and the underestimation decreases with the increase of far offset distances. For 30 m far offset distance, lowest underestimation is observed. Here, in case-II at a normalized array centre distance of 1, normalized Rayleigh wave velocity is found to reach below 0.9 specifically with the increased impedance scenario cases (Fig. 11c and d). Fig. 12 shows the near-field effects for Case-III S-wave velocity model, i.e. when a hard layer gets

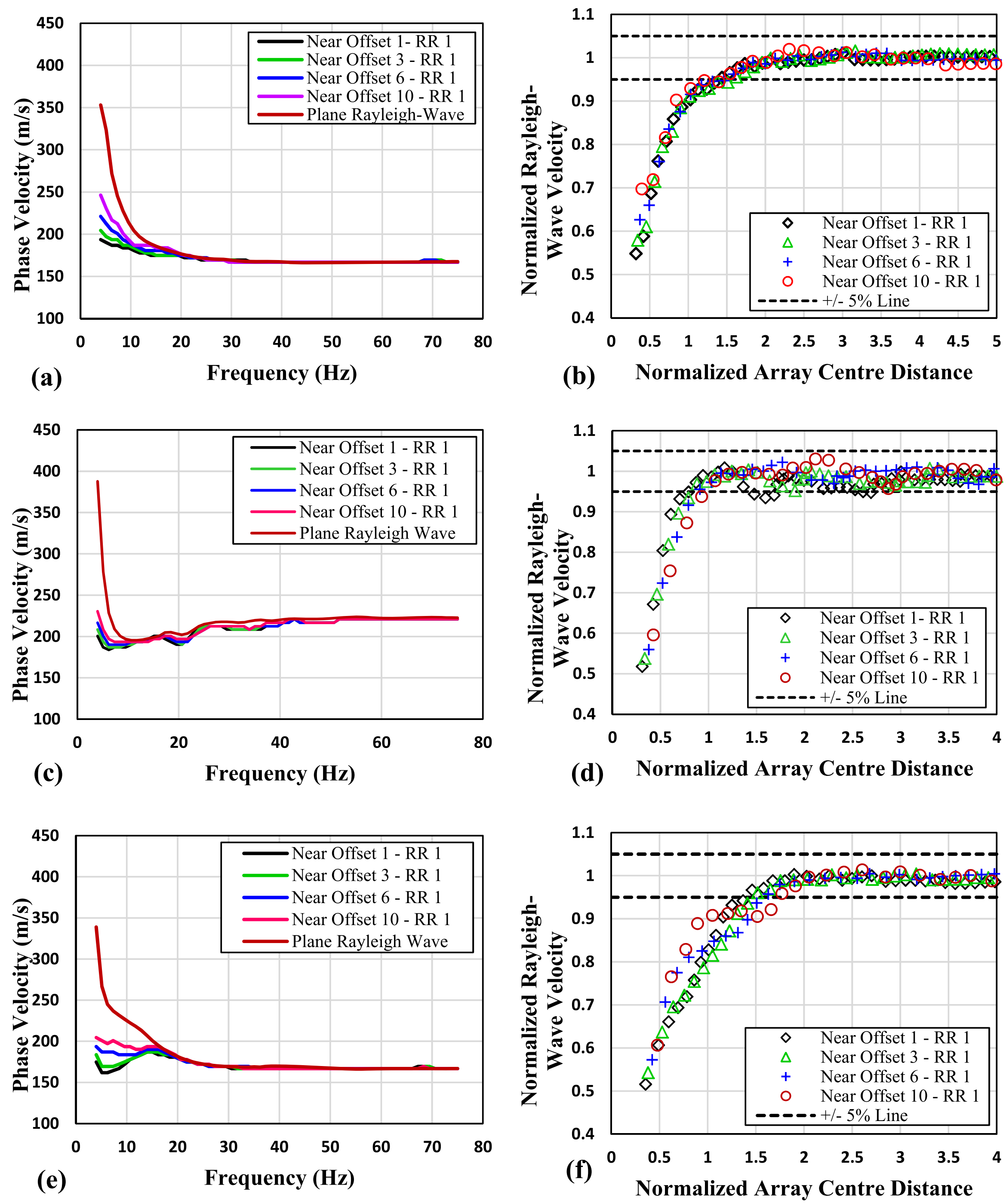

Fig. 13. Effect of near offset distances; Case-I(b): (a) Comparison of dispersion curves, (b) In terms of normalized parameters; Case-II(b): (c) Comparison of dispersion curves, (d) In terms of normalized parameters; and Case-III(b): (e) Comparison of dispersion curves, (f) In terms of normalized parameters.

trapped between two soft layers. Here also, very high underestimation is observed for high impedance contrast cases. In this case, it is observed that at a normalized array centre distance of ≥1.5, a better estimation of Rayleigh wave velocity is obtained for all the receiver cases.

The underestimation in Rayleigh wave phase velocity is quantified in terms of normalized Rayleigh wave velocity with respect to normalized array centre distance and has been presented in Table 5. From the Table 5 it is very much evident that at normalized array centre distance 1 for Case-III, i.e. inversely dispersive profile with trapped hard layer, is worst affected. Whereas Case-I and Case-II S-wave velocity models show a minimum underestimation of 0.9 and 0.86, respectively, but the Case-III S-wave velocity model exhibits a minimum underestimation of 0.84. At 1.5 normalized array centres distance, the underestimation becomes ≤10% irrespective of the type of S-wave velocity models, and Case-II S-wave velocity model show the maximum underestimation because of high data scatter.

To simulate the effect of near offset distances, four different near offset distances: 1 m, 3 m, 6 m and 10 m have been considered. Receiver-to-receiver (RR) distance is maintained as 1 m. To illustrate this effect, results for all the three profiles with bed-rock velocity 500 m/s [i.e. Case-I(b), Case-II(b) and Case-III(b)] with 30 m far offset are presented in Fig. 13a to f. Near offset distance largely affects the error due to near-field effects. Fig. 13a, c and e represent the results in

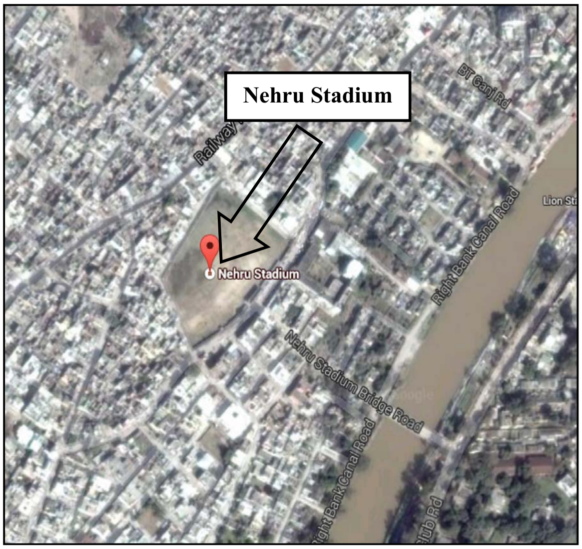

Fig. 14. Location of Nehru stadium site where active and passive source tests have been conducted.

terms of comparison of dispersion curves for different near offset distances with the plane Rayleigh wave dispersion curve for near offset and inter-receiver spacing equals to 1. Fig. 13b, d and f present the result in terms of normalized parameters. These results clearly show the improvement in the estimation of phase velocity with the increase in near receiver distances. The improvement is quite significant for normally dispersive shear wave velocity profile, which is quite distinguishable from normalized plots as well.

4. Experimental study

The findings of numerical simulations have been validated by experimental findings. For this purpose active and passive source tests have been conducted at the Nehru Stadium site in Roorkee city, India. The stadium is surrounded by several city roads, which are the good sources of passive energy at the middle of the ground. Fig. 14 shows the site location of Nehru Stadium ground. In experimental study, it is quite difficult to obtain the dispersion curve for plane Rayleigh wave. For this purpose, it is planned to carry out passive source tests to generate the reference plane Rayleigh wave dispersion curve. In passive source tests, while the energy comes from far away, and as the body waves attenuate faster than the surface waves, the propagating body waves die out, and the surface waves prevail. So, here passive surface wave tests are used for plane Rayleigh wave case and active source surface wave tests are used for the full-wave field case.

Active source tests have been conducted with McSeis-SXW 24 channel MASW set up (Fig. 15a) which is available in the Department of Earthquake Engineering, IIT Roorkee. Surface wave data are collected using 24 vertically mounted 2 Hz geophones with an 80 kg drop weight (Fig. 15b). The inter-receiver spacing was always maintained as 2 m. All the data are analyzed separately to generate the dispersion curve for that particular array configuration. Fig. 16a presents a sample recording trace with inter receiver and source to 1st receiver spacing of 2 m, and Fig. 16b shows the dispersion spectra obtained after the data analysis.

Passive surface wave test is also conducted using 2 Hz geophones. Two different kind of arrays have been used for this purpose: Linear array and L-shaped array. The array length of linear array is 46 m with a inter receiver spacing of 2 m. A total of 33 s of recording is taken with a total data points of 16,384. Total ten continuous sets of such records are captured with a total duration of 330 s. Further, the L-shape array is selected as it was difficult to identify the actual direction of passive energy. So, a 2D array is taken so as to capture the noise from any possible direction. The length of each side of 'L' is 20 m, which equals roughly to the actual depth of investigation. The spacing between two geophones have been kept 4 m, and each side of 'L' is formed by six geophones. In all, eleven number of geophones have been used in the testing. The data is analyzed using SPAC (Spatial Auto-Correlation) method. The details about the parameters used in the passive wave recordings are listed in Table 6. Fig. 17a and b present the dispersion spectra for Linear and L-shaped array, respectively. For both the arrays, a distinct spectra is obtained, while in L-shaped array, energy is not that distinct like Linear array beyond 20 Hz frequency. Once we got the two separate dispersion curves, we combined both the dispersion curves to generate a single dispersion curve and then used this as plane Rayleigh wave curve to express the near-field effects in terms of normalized parameters.

Fig. 18a shows the comparison of dispersion curves of active test with passive test dispersion curve for different near offset distances, and Fig. 18b presents the near-field effects in terms of normalized parameters. Passive test dispersion curve, which basically represents the plane Rayleigh wave dispersion curve, exhibits the higher velocity than the active source dispersion curves. It clearly shows that with the increase of source-to-first receiver distance active tests velocity approaches towards the true Rayleigh wave velocity. The results show quite similarity with our numerical simulation and follow the similar trend. At normalized array centre distance >2, the error is $<10\%$ which supports the numerical findings of this study. Fig. 18c and d show the comparison of dispersion curves from active surface wave tests for different far offset distances with passive surface wave tests and near-field effects in terms of normalized parameters, respectively. Maximum underestimation is observed for the lower far offset distances, and as the far offset distances increase, the data shows quite smooth variation and lower underestimation. At normalized array

Fig. 15. (a) Data acquisition system McSeis-SXW 24 channel seismograph, and (b) Sample data acquisition at site with 80 kg drop weight.

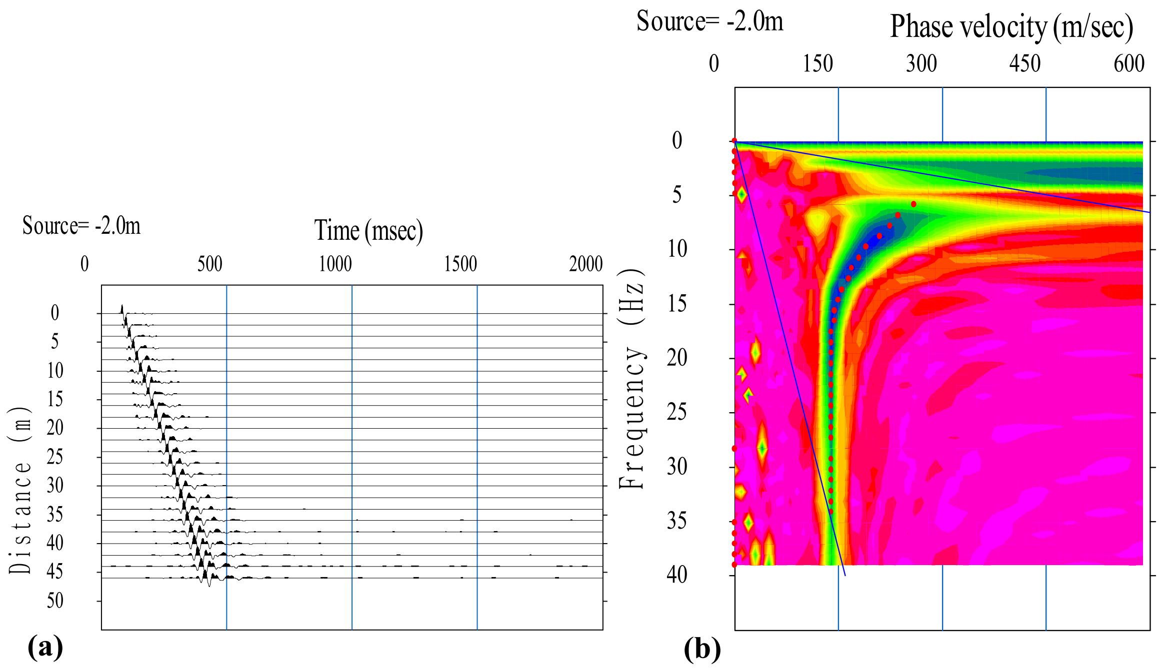

Fig. 16. Active MASW test; (a) Recorded trace, and (b) Generated dispersion spectra.

Table 6
Parameters used in the passive recording.

Linear Array		**L-Shaped array**	
No. of Channels	24	No. of Channels	11
Array Length	46 m	Side Length	20 m
Geophone Spacing	2 m	Geophone Spacing	4 m
Recording Time	~33 s	Recording Time	~33 s
Data Points	16,384	Data Points	16,384
Time step	0.002	Time step	0.002
Sampling Frequency	500	Sampling Frequency	500
Nyquist Frequency	250	Nyquist Frequency	250

centre distance > 1.5, the results show a reduced underestimation (< 10%), which holds well with our findings from numerical investigations.

5. Discussion

The above analysis clearly depicts the underestimation of Rayleigh wave phase velocity from numerical simulations and experimental studies. Far offset distances and type of S-wave velocity model seems to affect the underestimation significantly. Near offset distance is also a deciding factor in the underestimation. The underestimation is found quite severe for high impedance S-wave velocity models at lower normalized array centre distance. To get a more clear insight about the problem, the modal dispersion curves for all the considered high

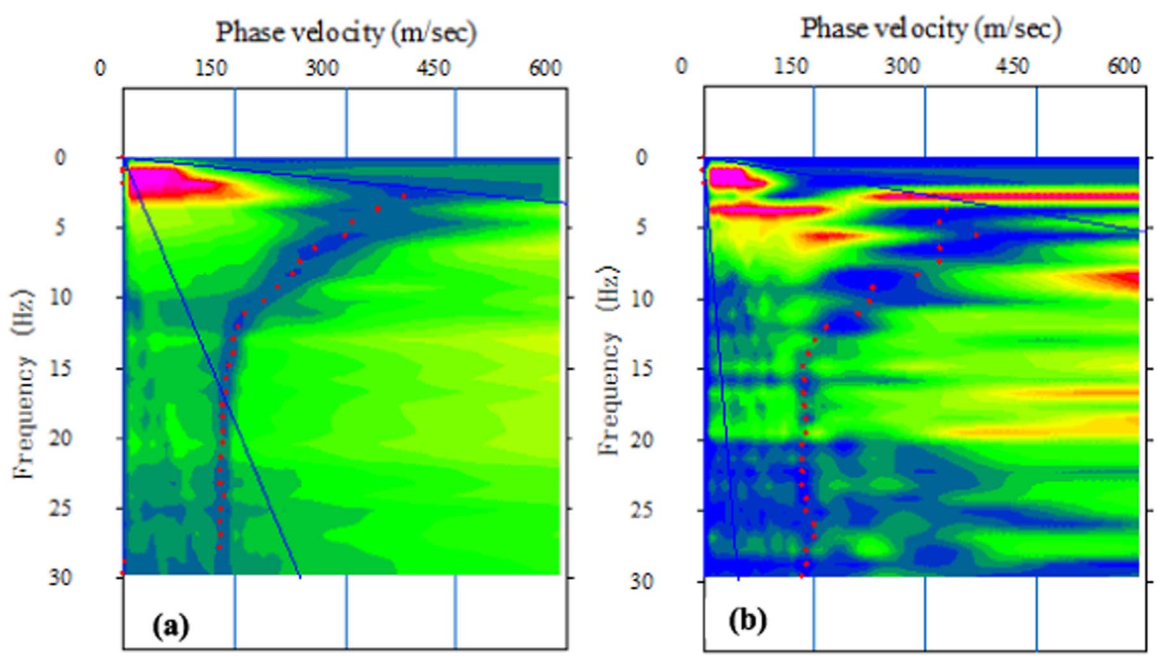

Fig. 17. Dispersion spectra for (a) Linear passive, and (b) L-shape passive tests.

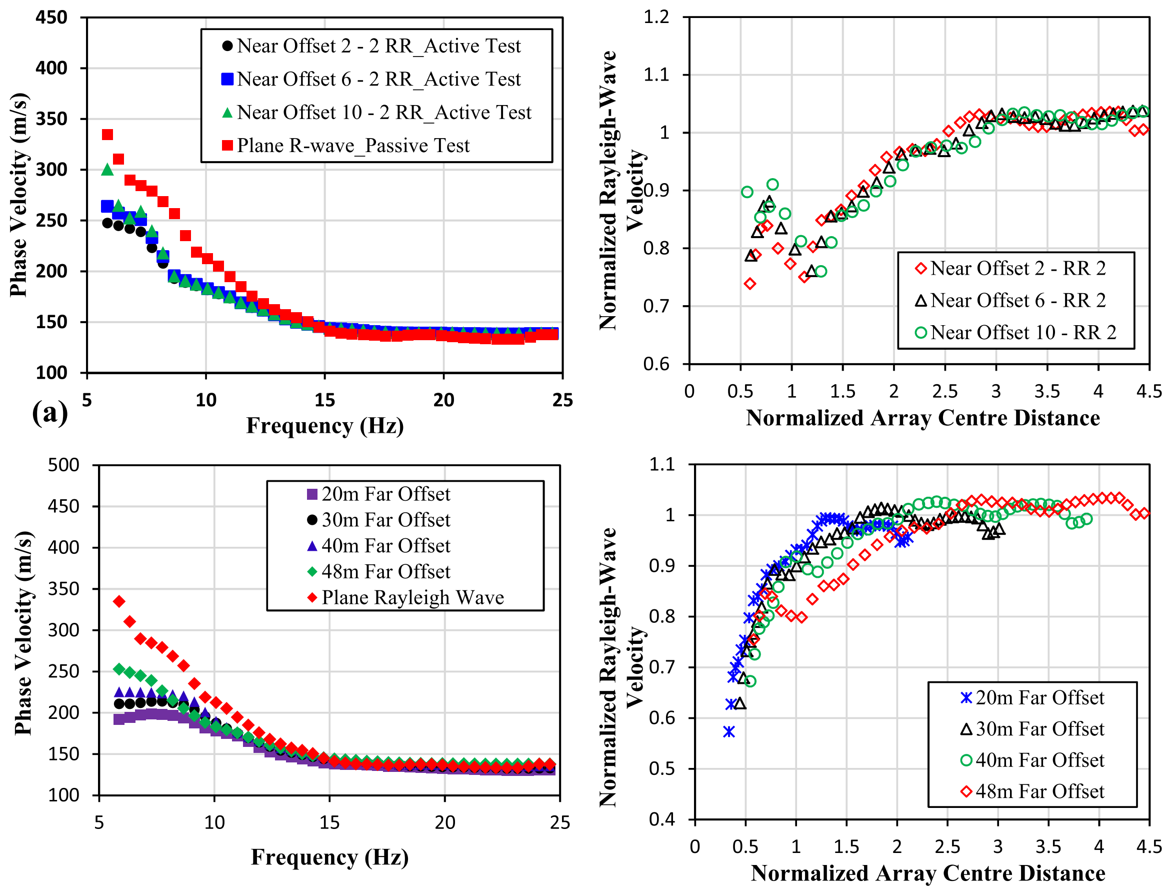

Fig. 18. Results from field tests for different near offset distance: (a) comparison of active and passive test dispersion curves, and (b) Near-field effects in terms of normalized parameters; For different far offset distances: (c) comparison of active and passive test dispersion curves, and (d) Near-field effects in terms of normalized parameters.

impedance S-wave velocity model cases are plotted with the respective effective phase velocity dispersion curves and PLAXIS simulated dispersion curves of 30 m far offset distance. Modal dispersion curves (fundamental and higher modes) have been generated using Thomson [28] and Haskell [7] algorithm later modified by Dunkin [6] and Knopoff [14]. An interesting result is observed for high impedance S-wave velocity models. Fig. 19 shows the superimposed modal dispersion curves, effective dispersion curves and PLAXIS simulated dispersion curves for Case-I(c) & (d) [Fig. 19a and b], Case-II(c) & (d) [Fig. 19c and d], Case-III(c) & (d) [Fig. 19e and f], i.e. half-space velocity of 700 m/s and 1000 m/s cases of considered three types of profiles. From Fig. 19a to f it is quite evident that for all the high impedance cases except Case-III(c) the effective phase velocity dispersion curves show a jump towards the first higher mode at the lowest frequency, i.e. 4 Hz. But the dispersion curves for full wave field, i.e. PLAXIS simulated dispersion curves using 30 receivers are unable to exhibit such kind of jump at lowest frequency due to the poor resolution in the dispersion spectra causing the severe underestimation. Usual practice in engineering site characterization using limited far offset distances and lower normalized array centre distance may lead to a velocity profile far away from the actual one for the sites where sharp impedance contrast exists. So, specifically for near bedrock situation, when a sharp impedance contrast is there attention must be paid at the lower frequency information, otherwise it may lead to the extraction of velocity profile which may be far away from the actual one.

6. Conclusions

Measurement of phase velocity of Rayleigh wave using MASW may get underestimated by the near-field effects. This study gives a clear insight about the discrepancies in the measurement of Rayleigh wave phase velocity due to near-field effects for different types of S-wave velocity models with varying impedance scenarios. Both the numerical and the field study clearly identify the underestimation of phase velocity at lower frequencies, and the underestimation exhibits a strong correlation with the normalized array centre distance. From the analysis the following conclusions can be drawn:

1. Near-field effects result in underestimation of the Rayleigh wave phase velocity and sometimes a little overestimation is also observed. Impedance contrast, i.e., different half-space velocity, is having a significant impact on the near-field effects. With the increase in impedance contrast, the underestimation seems to increase at lower normalized array centre distances (< 0.5) for all the considered three types of S-wave velocity models. This is because of occurrence of mode jump with the increase in impedance contrasts. However this mode jump is difficult to observe with limited far offset distances.
2. The simulation is performed for different far offset distance configurations, and it is found that far offset distances is also one of the prominent deciding factors. Higher the far offset distances, lower is the underestimation. So, by increasing the far offset distances underestimation can be reduced to some extent.
3. Type of S-wave velocity model influences the near-field effects significantly. Inversely dispersive S-wave velocity models shows more prominent near-field effects with a large data scatter in comparison to normally dispersive profile. In case of normally dispersive profile, the underestimation can be reduced below 10% for a normalized array Centre distance of 1. However, a normalized array centre distance of 1.5 or more is required for invasively dispersive profiles to reduce the underestimation below this level

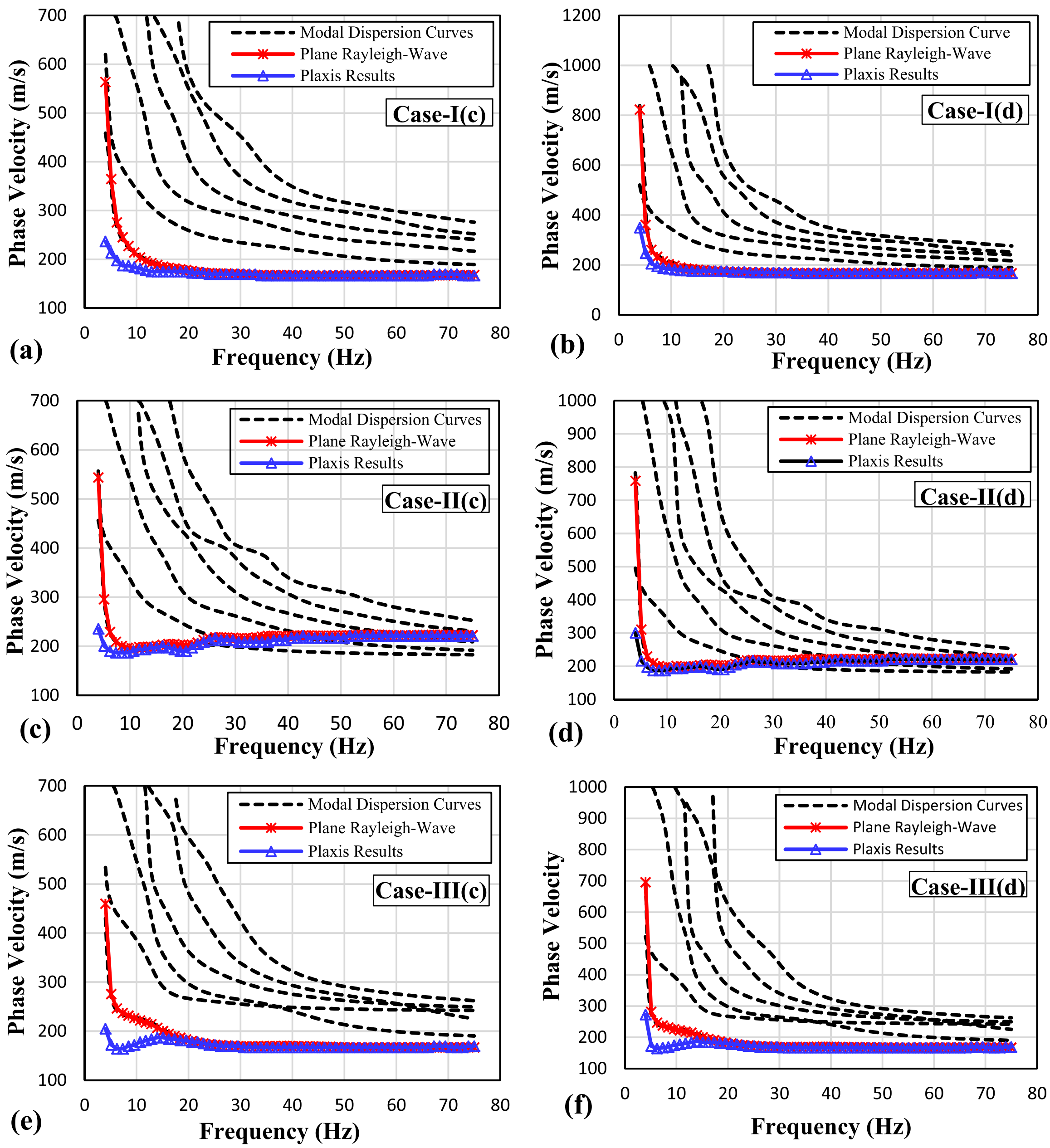

Fig. 19. Comparison of modal dispersion curves with plane Rayleigh wave dispersion curve and PLAXIS simulated dispersion curves.

(i.e 10%). It is observed that at a normalized array centre distance of 2, the underestimation is reduced below 5% irrespective of S-wave velocity models and impedance contrasts.

4. Near offset distance also influences the error due to near-field effects. Analysis shows that increasing the near offset distance, significant improvement is observed for normally dispersive profile but little less improvement is observed for both the inversely dispersive profiles. But in overall, underestimation decreases with the increase in near offset distance.
5. To simulate the near-field effects experimentally, field active and passive tests have been conducted. As it is quite difficult to obtain the dispersion curve for pure plane Rayleigh wave in field, passive test results are used as an approximation. Plane Rayleigh wave dispersion curve (dispersion curve from passive test) shows the higher phase velocity in comparison with all other active test dispersion curves, which clearly depicts the underestimation of phase velocity in the case of an active surface wave field test.
6. Experimental findings also support the outcome of our numerical investigations and both the results are in good agreement. Field tests results show similar trends in terms of normalized parameters as well. For different far offset distances at a normalized array centre distance >2, the error is $<10\%$ which supports the numerical findings of this study. For different near offset distances, at a normalized array centre distance >2, the error is $\leq 10\%$ which also holds well with our numerical simulations.

Acknowledgement

We are very thankful to the anonymous reviewers for their valuable suggestions, which helped us to improve the manuscript significantly. We are also thankful to Prof. H.R. Wason for his encouragement and guidance during the initial course of study. Financial support received from the SERB/DST, Government of India under Young Scientist Scheme (No. SB/FTP/ETA-164/2014) has also been acknowledged.

References

[1] Aung AMW, Leong EC. Discussion of near-field effects on array-based Surface wave methods with active sources by S. Yoon and G. J. Rix. J Geotech Geoenviron Eng 2010;136:773–5.

[2] Aung AMW, Leong EC. Finite-Element modeling of continuous surface waves tests: numerical accuracy with respect to domain Size. J Geotech Geoenviron Eng 2011;137:1294–8.

[3] Boaga J, Vignoli G, Cassiani G. Shear wave profiles from surface wave inversion: the impact of uncertainty on seismic site response analysis. J Geophys Eng 2011;8:162–74.

[4] Bodet L, Abraham O, Clorennec D. Near-offset effects on Rayleigh-wave dispersion measurements: physical modelling. J Appl Geophys 2009;68:95–103.

[5] Brinkgreve RBJ. Plaxis 2-D version 8.2. Lisse: A.A. Balkema Publisher; 2002.

[6] Dunkin JW. Computation of modal solution in layered elastic media at high frequencies. Bull Seismol Soc Am 1965;55:335–58.

[7] Haskell NA. The dispersion of surface waves on multilayered media. Bull Seismol Soc Am 1953;43(1):17–34.

[8] Heisey JS, Stokoe KH, Meyer AH. Moduli of pavement system from spectral analysis of surface wave (Transportation Research Record 852, TRB). National Research Council; 1982. p. 22–31.

[9] Hiltunen D, Woods R. Variables affecting the testing of pavement by the surface wave method (Transportation Research Record 1260). Washington, D.C.: Transportation Research Board, National Research Council; 1990. p. 42–52.

[10] Foti S, Comina C, Boiero D, Socco LV. Non-uniqueness in surface-wave inversion and consequences on seismic site response analyses. Soil Dyn Earthq Eng 2009;29:982–93.

[11] Gucunski N, Woods RD. Numerical simulation of the SASW test. Soil Dyn Earthq Eng 1992;11:213–27.

[12] Jakka RS, Roy N, Wason HR. Implications of surface wave data measurement uncertainty on seismic ground response analysis. Soil Dyn Earthq Eng 2014;61–62:239–45.

[13] Jones RB. In-situ measurement of the dynamic properties of soil by vibration methods. Geotechnique 1958;8(1):1–21.

[14] Knopoff L. A matrix method for elastic wave problems. Bull Seismol Soc Am 1964;54:431–8.

[15] Lai CG. Simultaneous inversion of Rayleigh phase velocity and attenuation for near-surface site characterization (Ph.D. dissertation). Georgia Institute of Technology; 1998. p. 370.

[16] Li J, Rosenblad BL. Experimental study of near-field effects in multichannel array-based surface wave velocity measurements. Near-Surf Geophys 2011;9(4):357366.

[17] Lysmer J, Kuhlemeyer RL. Finite dynamic model for infinite media. ASCE J Eng Mech Div 1969;95(4):859–77.

[18] Miller RD, Xia J, Park CB, Ivanov J. Using MASW to map bedrock in Olathe. Kans Soc Explor Geophys 1999:433–6.

[19] Nazarian S, Stokoe KH-II, Hudson WR. Use of spectral analysis of surface waves method for determination of moduli and thicknesses of pavement systems. Transp Res Rec 1983;930:38–45.

[20] O'Neill A. Seismic surface waves special issue, guest editorial. J Environ Eng Geophys 2005;10(2):65–72.

[21] Park CB, Miller RD, Xia J. Multi-channel analysis of surface waves. Geophysics 1999;64(3):800–8.

[22] Rix GJ, Lai CG, Foti S. Simultaneous measurement of surface wave dispersion and attenuation curves. Geotech Test J 2001;24(4):350–8.

[23] Roberts J, Asten M. A study of near source effects in array-based (SPAC) microtremor surveys. Geophys J Int 2008;174(1):159–77.

[24] Roy N, Jakka RS, Wason HR. Effect of surface wave inversion non-uniqueness on 1-d seismic ground response analysis. Nat Hazards 2013;68(2):1141–53.

[25] Sanchez-Salinero I. Analytical investigation of seismic methods used for engineering applications (Ph.D. dissertation). Austin: Univ. of Texas; 1987.

[26] Socco LV, Strobbia C. Surface-wave method for near-surface characterization: a tutorial. Near Surf Geophys 2004;2(4):165–85.

[27] Strobbia C, Foti S. Multi-offset phase analysis of surface wave data (MOPA). J Appl Geophys 2006;59:300–13.

[28] Thomson WT. Transmission of elastic waves through a stratified solid medium. J Appl Phys 1950;21(1):89–93.

[29] Wathelet M. An improved neighborhood algorithm: parameter conditions and dynamic scaling. Geophys Res Lett 2008;35:L09301. http://dx.doi.org/10.1029/2008GL033256.

[30] Xia J, Miller RD, Park CB. Estimation of near-surface shear-wave velocity by inversion of Rayleigh wave. Geophysics 1999;64(3):691–700.

[31] Xu Y, Xia J, Miller RD. Quantitative estimation of minimum offset for multichannel surface-wave survey with actively exciting source. J Appl Geophys 2006;59:117–25.

[32] Yoon S. Array-based measurement of surface wave dispersion and attenuation using frequency-wave number analysis (Ph.D. dissertation). Atlanta, Ga: Georgia Institute of Technology; 2005.

[33] Yoon S, Rix GJ. Near-field effects on array-based surface wave methods with active sources. J Geotech Geoenviron Eng 2009;135:399–406.

[34] Zywicki DJ. Advanced signal processing methods applied to engineering analysis of seismic surface waves (Ph.D. thesis). Atlanta, USA: Georgia Institute of Technology; 1999.

[35] Zywicki DJ, Rix GJ. Mitigation of near-field effects for seismic surface wave velocity estimation with cylindrical beamformers. J Geotech Geoenviron Eng 2005;131:970–7.

Further reading

[1] Rix G, Computer programs for surface wave analysis. (⟨http://geosystems.ce.gatech.edu/soil_dynamics/research/surfacewavesanalysis/⟩).